Trapped, Two-Armed, Nearly Vertical Oscillations in Polytropic Disks

Shoji KATO

2-2-2 Shikanodai, Ikoma-shi, Nara, Japan 630-0114
email: kato.shoji@gmail.com
(to be published in PASJ 62, No.3, 2010)

Abstract

We have examined trapping of two-armed nearly vertical oscillations in polytropic disks. Two-armed nearly vertical oscillations are interesting in the sense that they are trapped in an inner region of disks with proper frequencies, if the inner edge of disks is a boundary that reflects oscillations. The frequencies of the trapped oscillations cover the frequency range of kHz QPOs to low frequency QPOs in LMXBs, depending on the modes of oscillations. Low frequency trapped oscillations are particularly interesting since their trapped region is wide. These low frequency oscillations are, however, present only when $\Gamma(\equiv 1+1/N)$ is close to but smaller than $4/3$ (when spin parameter a_* is zero), where N is the polytropic index. The above critical value $4/3$ slightly increases as a_* increases.

1 Introduction

One of the possible candidates of high-frequency quasi-periodic oscillations (HFQPOs) observed in low-mass X-ray binaries is resonantly excited p- and/or g-mode oscillations in deformed disks (Kato 2004, 2008a,b; Ferreira and Ogilvie 2008; Oktariani et al. 2010). The disk deformation required in this model is a warp or an eccentric deformation in equatorial plane. Recent numerical MHD simulations (Henisey et al. 2009) seem to have preliminary confirmed the presence of the excitation mechanism.

The high frequency QPOs observed in black-hole candidates appear in pairs with frequency ratio of 3 : 2. This characteristic of high-frequency QPOs in black-hole candidates seems to be described by the above model, if we assume that geometrically thin disks are surrounded by hot tori and that the QPOs photons are disk photons Comptonized in the tori (Kato and Fukue 2006). The twin kHz QPOs observed in neutron stars, on the other hand, have always not the 3 : 2 frequency ratio. They change their frequencies with time with correlation. If we want to describe such characteristics of kHz QPOs by the above model, a warp or eccentric disk deformation must have a time-dependent precession. In the case of neutron stars, distinct from the case of black holes, such precession of the deformation might be expected, since the central stars have surfaces and this might become causes of time-dependent precession through magnetic and radiative couplings between the central sources and the disks. It is not clear, however, whether possible time-dependent precession of deformation has a time scale consistent with the time variations of the kHz QPOs.

In this context, it is worthwhile examining whether there are other kinds of disk deformations that can become a possible source of resonant excitation of high-frequency oscillations in disks. This problem has been examined by Kato (2009), and it was suggested that two-armed nearly vertical oscillations[1] can excite high-frequency p- and/or g-mode oscillations. Hence, it will be interesting to examine whether there are two-armed nearly vertical oscillation modes that can become a global deformation of disks.

More interestingly, the two-armed vertical disk oscillations themselves may be origins of the varous types of QPOs observed in neutron-star LMXBs. This is because two-armed nearly vertical osillations occur in the inner region of disks and cover a wide range of frequency by difference of modes.

Based on these considerations, we examine in this paper basic properties of the two-armed vertical disk oscillations. That is, we examine their characteristics of trapping, eigen-frequency and its dependence on polytropic index specifying the vertical disk structure, using the mathematical formulations already prepared by Silbergleit et al. (2001) to study the trapping of the corrugation waves (c-mode oscillations).

2 Overview of Trapping of Two-Armed Vertical Oscillations in Polytropic Disks

Before having a rough image of nearly vertical oscillations in vertically polytropic disks, we briefly mention nearly vertical oscillations in isothermal disks, because it is instructive to have a rough image of wave trapping in disks.

If a disk oscillation with azimuthal wavenumber m occur isothermally and locally in vertical direction in isothermal disks, the frequency, ω, is given by (see, e.g., Okazaki et al. 1987)

$$(\omega - m\Omega)^2 - n\Omega_\perp^2 = 0, \qquad (1)$$

where n denotes the node number ($n = 1, 2, ...$) of the oscillations in the vertical direction, and Ω and $\Omega_\perp$ are, respectively, the angular velocity of disk rotation at the radius in consideration and the vertical epicyclic frequency at the radius. The oscillations are, however, cannot be purely vertical by inhomogeneity of the disk in the radial direction. They essentially have horizontal velocity components. In other words, the vertical oscillations described by equation (1) are not rigorous. The vertical oscillations couple with purely horizontal inertial oscillations, $(\omega - m\Omega)^2 - \kappa^2 = 0$, through pressure. If the coupling is considered with local approximations in the radial direction, we have a dispersion relation, which is written as (Okazaki et al. 1987)

$$[(\omega - m\Omega)^2 - \kappa^2][(\omega - m\Omega)^2 - n\Omega_\perp^2] = c_s^2 k^2 (\omega - m\Omega)^2, \qquad (2)$$

---

[1] There will be no commonly accepted classification and terminology concerning disk oscillations. Here, we classify oscillations into four types, i.e., p-mode, g-mode, c-mode and vertical p-mode oscillations (see, for example, Kato 2001; Kato et al. 2008). The oscillations considered here are the vertical p-mode oscillations.

where $c_{\rm s}$ is the acoustic speed, κ is the horizontal epicyclic frequency, and k is the horizontal wavenumber of the oscillations.

Since we are now interested in nearly vertical oscillations, i.e., $(\omega - m\Omega)^2 - n\Omega_\perp^2 \sim 0$ ($n = 1$, 2, 3,...), equation (2) shows that their propagation region in the radial direction is described by

$$(\omega - m\Omega)^2 - n\Omega_\perp^2 \geq 0, \qquad (3)$$

since $\Omega_\perp$ is always larger than κ.

We now proceed to polytropic disks with barotropic gas with polytropic index N, i.e., $p \propto \rho^{(1+1/N)}$, where p and ρ are pressure and density, respectively. The frequency, ω, of purely vertical oscillations is then given by (Silbergleit et al 2001, Kato 2005)

$$(\omega - m\Omega)^2 - \Psi_n \Omega_\perp^2 = 0, \qquad (4)$$

where Ψ_n is

$$\Psi_n = \left\{ \begin{array}{lll} 1 & \text{for} & n = 1 \\ 2 + 1/N & \text{for} & n = 2 \\ 3 + 3/N & \text{for} & n = 3. \end{array} \right. \qquad (5)$$

The case of isothermal disks corresponds to $N = \infty$.

In oscillations of $n = 1$, $\omega - m\Omega$ is independent of N, but in oscillations of $n \neq 1$ it depends on N. That is , for two-armed oscillations ($m = 2$), equation (4) has solution given by

$$\omega = 2\Omega - (1 + \Gamma)^{1/2}\Omega_\perp \qquad \text{for} \quad n = 2 \qquad (6)$$

and

$$\omega = 2\Omega - (3\Gamma)^{1/2}\Omega_\perp \qquad \text{for} \quad n = 3, \qquad (7)$$

where $\Gamma = 1 + 1/N$, and Γ is usually in the range of $\Gamma = 1 \sim 5/3$. An interesting result shown in equation (7) is that oscillations with $n = 3$ can have low-frequencies for reasonable values of Γ.

As in the case of isothermal disks, the nearly vertical oscillations are also not localized at a particular radius. They propagate in the radial direction. The propagation region is specified, as in the case of isothermal disks, by (see section 4 for details)

$$(\omega - m\Omega)^2 - \Psi_n\Omega_\perp^2 \geq 0. \qquad (8)$$

The propagation diagram showing the propagation region of the oscillations in the radial direction is given in figure 1 for oscillations with $n = 1$ and 2, and in figure 2 for oscillations with $n = 3$. As the value of n increases, the propagation region of oscillations becomes narrower in the frequency - radius plane (i.e., propagation diagram), and finally for oscillations with $n = 3$, the propagation region in the inner region of disks disappears for oscillations with $\Gamma > 4/3$.

The next problem is to examine where the oscillations are really trapped and how much the frequency of the trapped oscillations is. To examine this problem, a careful treatment of the wave equation is necessary and this is done

3

in the subsequent sections. Here, however, in order to have a rough image of trapping, we discuss qualitatively what determines the frequency of the trapped oscillations.

Let us assume tentatively that the frequency of the trapped oscillation is ω and the outer boundary of the trapped region is r_c. The inner boundary of the trapped region, r_i, is taken at the inner edge of the disks, which is $3r_g$ when the central source has no spin, r_g being the Schwarzschild radius. Then, roughly speaking, $r_c - r_i$ must be on the order of the wavelength of the trapped oscillations. If some kinds of mean values of $(\omega - m\Omega)^2 - \kappa^2$ and c_s^2 in the trapped region are denoted, respectively, $\langle (\omega - m\Omega)^2 - \kappa^2 \rangle$ and $\langle c_s^2 \rangle$, then the trapping condition is $\langle (\omega - m\Omega)^2 - \kappa^2 \rangle \sim \langle c_s^2 \rangle / (r_c - r_i)^2$ (for the fundamental mode in the radial direction), since oscillations propagate in the radial direction as inertial acoustic waves. This trapping condition is realized only when ω has a particular value, say ω_t. This is because for $\omega > \omega_t$, $\langle (\omega - m\Omega)^2 - \kappa^2 \rangle (r_c - r_i)^2$ is too small compared with $\langle c_s^2 \rangle$, since the width of the propagation region, i.e., $r_c - r_i$, is too narrow (see figures 1 and 2). On the other hand, for $\omega < \omega_t$, the value of $\langle (\omega - m\Omega)^2 - \kappa^2 \rangle (r_c - r_i)^2$ becomes larger than $\langle c_s^2 \rangle$, since the width, $r_c - r_i$, becomes too large. To know the detailed value of ω_t for the trapping, we must make numerical calculations, as is done in the subsequent sections.

At this stage, without detailed numerical calculations, we can say that when Γ is large, the frequency of the trapped oscillations is low, if other parameters, including the radial distribution of c_{s0} in disks, are fixed (see figure 4). Let us assume that the trapping condition has satisfied for a frequency, say ω_t, when Γ has a value, say Γ_t. If Γ increases from Γ_t, r_c and thus $r_c - r_i$ decreases from the value in the above case, if the frequency ω is fixed at ω_t [see equations (6) and (7) and curves in figures 1 and 2]. Thus, the trapping condition is not satisfied at $\omega = \omega_t$. For the trapping condition to be satisfied we must increase the width of the trapping region. This can be done by decreasing ω from ω_t.

3 Unperturbed Disks and Equations Describing Disk Oscillations

3.1 Basic Assumptions and Unperturbed Disks

We consider geometrically thin, relativistic disks. For mathematical simplicity, however, the effects of general relativity are taken into account only when we consider radial distributions of $\Omega(r)$, $\kappa(r)$, and $\Omega_\perp(r)$. They are, in turn, the angular velocity of disk rotation, the epicyclic frequencies in the radial and vertical directions. Except for them, the Newtonial formulations are adopted. Since geometrically thin disks are considered, Ω, is approximated to be the relativistic Keplerian angular velocity, $\Omega_K(r)$, when its numerical values are necessary. Here, r is the radial coordinate of cylindrical ones (r, φ, z), where the z-axis is perpendicular to the disk plane and its origin is the disk center. Functional forms of $\Omega_K(r)$, $\kappa(r)$, and $\Omega_\perp(r)$ are given in many literature sources (e.g., Kato et al. 2008)

4

The disks are assumed to consist of a barotropic gas with polytropic index N, i.e., the pressure p and density ρ are related by $p \propto \rho^{(N+1)/N}$. The hydrostatic balance in the vertical direction then gives (e.g., Kato et al. 2008)

$$\rho_0(r,z) = \rho_{00}(r)\left(1 - \frac{z^2}{H^2}\right)^N, \tag{9}$$

$$p_0(r,z) = p_{00}(r)\left(1 - \frac{z^2}{H^2}\right)^{1+N}, \tag{10}$$

where subscript 0 represents the quantities in the equilibrium state and 00 are those on the equatorial plane. The acoustic speed defined by $c_{\mathrm{s}}^2 = \Gamma dp_0/d\rho_0$ is also given by

$$c_{\mathrm{s}}^2(r,z) = c_{\mathrm{s}0}^2(r)\left(1 - \frac{z^2}{H^2}\right), \tag{11}$$

where Γ is related to N by $\Gamma = (N+1)/N$ or $N = 1/(\Gamma - 1)$. The hydrostatic balance in the vertical direction also shows that the half-thickness H of disks is related to $c_{\mathrm{s}0}$ and $\Omega_\perp$ by

$$\Omega_\perp^2 H^2 = 2N c_{\mathrm{s}0}^2. \tag{12}$$

3.2 Equations Describing Disk Oscillations

We consider small-amplitude perturbations in the above disk. The perturbations are assumed to be proportional to $\exp[i(\omega t - m\varphi)]$, where ω and m are frequency and azimuthal wavenumber, respectively, of the perturbations. Then, hydrodynamical equations describing them are (e.g., Kato et al. 2008)

$$i\tilde{\omega}\rho_1 + \frac{\partial}{r\partial r}(r\rho_0 u_r) - i\frac{m}{r}\rho_0 u_\varphi + \frac{\partial}{\partial z}(\rho_0 u_z) = 0, \tag{13}$$

$$i\tilde{\omega}u_r - 2\Omega u_\varphi = -\frac{\partial h_1}{\partial r}, \tag{14}$$

$$i\tilde{\omega}u_\varphi + \frac{\kappa^2}{2\Omega}u_r = i\frac{m}{r}h_1, \tag{15}$$

$$i\tilde{\omega}u_z = -\frac{\partial h_1}{\partial z}, \tag{16}$$

where h_1 and $\tilde{\omega}$ are defined, respectively, by

$$h_1 = \frac{p_1}{\rho_0} = c_{\mathrm{s}}\frac{\rho_1}{\rho}, \tag{17}$$

$$\tilde{\omega} = \omega - m\Omega. \tag{18}$$

Here, (u_r, u_φ, u_z), p_1, and ρ_1 are the Eulerian velocity, pressure, and density perturbations over the unperturbed ones, respectively. Equation (13) is the equation of continuity, equations (14) – (16) are in turn the r-, φ-, and z-components of equation of motion.

Elimination of u_r, u_φ, u_z, and ρ_1 from equations (13) – (17) leads to a partial differential equation of h_1. In the processes, we neglect the radial variations of the unperturbed density and some other quantities, assuming that their characteristic radial scales are longer than the characteristic radial wavelength of the perturbations. Then, we have an equation describing the variation of h_1 in the form:

$$\frac{1}{\tilde{\omega}} \frac{\partial}{\partial r} \left(\frac{\tilde{\omega}}{\tilde{\omega}^2 - \kappa^2} \frac{\partial h_1}{\partial r} \right) + \frac{1}{\tilde{\omega}^2} \frac{1}{\rho_0} \frac{\partial}{\partial \rho_0} \frac{\partial}{\partial z} \left(\rho_0 \frac{\partial h_1}{\partial z} \right) + \frac{1}{c_s^2} h_1 = 0. \qquad (19)$$

As is clear from the derivation processes, this equation is obtained under the framework of the Newtonian hydrodynamics. A fully general relativistic one corresponding to equation (19) has been derived by Perez et al. (1997) and used by Silbergleit et al. (2001, 2008). In their equation the factor $\tilde{\omega}$ inside and the factor $1/\tilde{\omega}$ outside the first r-derivative $\partial/\partial r$ in the first term on the right-hand side of equation (19) are absent. However, relativistic factors related to metric appear in the first and third terms of equation (19). These factors are on the order of unity, but not unity. For example, on the first term of equation (19), a metric factor $g^{rr}(r)$ is multiplied, which is $2/3$ at $3r_g$ (r_g being the Schwarzschild radius) in the case of the Schwarschild metric.

In this paper we do not take into account the relativistic effects except the functional forms of Ω, κ and $\omega_\perp$ as mentioned before and start from equation (19). In the case of the polytropic gas mentioned in subsection 3.1, by changing the independent variables from (r, z) to (r, η), where $\eta = z/H$, we can reduce equation (19) to

$$\tilde{\omega} H^2 \frac{\partial}{\partial r} \left(\frac{\tilde{\omega}}{\tilde{\omega}^2 - \kappa^2} \frac{\partial h_1}{\partial r} \right) + \frac{1}{(1 - \eta^2)^N} \frac{\partial}{\partial \eta} \left[(1 - \eta^2)^N \frac{\partial h_1}{\partial \eta} \right] + \frac{\tilde{\omega}^2 H^2}{c_{s0}^2} \frac{1}{1 - \eta^2} h_1 = 0. \qquad (20)$$

The assumption of strong variation of perturbations in the radial direction ensures the WKB separability of variable in the above partial differential equation in the form of $h_1(r, \eta) = \tilde{h}_1(r) g(r, \eta)$. Here, the function g varies slowly with r. Extensive studies of disk oscillations by the WKB procedures have been made by Wagoner and his collaborators, e.g., Nowak and Wagoner (1992), Perez et al. (1997), Silbergleit et al. (2001). Here, we follow the procedures of Silbergleit et al. (2001) used to study trapped c-mode oscillations, although notations adopted here somewhat different from theirs.

By using the decomposition of $h_1(r, z)$ mentioned above, we can reduce equation (20) into the following set of two ordinary differential equations (Silbergleit et al. 2001):

$$\frac{1}{(1 - \eta^2)^N} \frac{d}{d\eta} \left[(1 - \eta^2)^N \frac{dg}{d\eta} \right] + \frac{\tilde{\omega}^2 H^2}{c_{s0}^2} \frac{1}{1 - \eta^2} g - 2NKg = 0, \qquad (21)$$

and

$$\tilde{\omega} H^2 \frac{d}{dr} \left[\frac{\tilde{\omega}}{\tilde{\omega}^2 - \kappa^2} \frac{d\tilde{h}_1}{dr} \right] + 2NK\tilde{h}_1 = 0, \qquad (22)$$

where $2NK$ is the separation constant. Since the term $\tilde{\omega}^2 H^2/c_{s0}^2$, which is equal to $2N\tilde{\omega}^2/\Omega_\perp^2$, in equation (21) weakly depends on r, g cannot be a function of η

6

alone, implying that both g and K also depend weakly on r. Taking these weak radial dependences of g and K into account as a perturbation, we solve equations (21) and (22) as eigen-value problems, following Silbergleit et al. (2001).

4 Eigen-Value Problems

First we consider the vertical eigen-value problems. Next, the eigen-value problems in the radial direction are considered.

4.1 Vertical Eigen-Value Problems

First, we solve vertical eigen-value problem, using equation (21). Since we are considering the oscillations where the vertical motions predominate over horizontal ones, we can take K to be zero in the lowest order of approximations (Silbergleit et al. 2001), and neglect the radial dependence of $\tilde{\omega}^2 H^2 / c_{s0}^2$, adopting its value at a radius, say r_c. Then, equation (21) leads to

$$(1 - \eta^2)\frac{d^2 g}{d\eta^2} - 2N\eta\frac{dg}{d\eta} + 2N\left(\frac{\tilde{\omega}^2}{\Omega_\perp^2}\right)_c g = 0, \tag{23}$$

where the subscript c denoted the value at the radius r_c. At this stage, r_c is arbitrary, but later, it is determined by an eigen-value problem in the radial direction. The results show that r_c can be regarded as the outer capture radius of the oscillations.

Equation (23) is solved as an eigen-value problem with the boundary condition $g(\pm 1) < \infty$. The eigenfunctions are then given by the Gegenbauer polynomials, C_n^λ (where $n = 1, 2, 3...$), i.e.,

$$g(\eta) = C_n^\lambda(\eta) \tag{24}$$

and the eigenvalues are specified by

$$2N\left(\frac{\tilde{\omega}^2}{\Omega_\perp^2}\right)_c = n(n + 2\lambda), \tag{25}$$

where n is the positive integer specifying the node number of g and

$$\lambda = N - \frac{1}{2}. \tag{26}$$

Equations (25) and (26) lead to

$$\tilde{\omega}_c^2 = \Psi_n \Omega_{\perp c}^2, \tag{27}$$

where Ψ_n is given by equation (5), and equation (27) is nothing but relation (4) at the capture radius. The explicit form of g is

$$g(\eta) \propto \begin{cases} \eta & \text{for} \quad n = 1 \\ 1 - (1 + 2N)\eta^2 & \text{for} \quad n = 2 \\ \eta - (1 + 2N/3)\eta^3 & \text{for} \quad n = 3. \end{cases} \tag{28}$$

7

Next, a small radial variation of $\tilde{\omega}^2/\Omega_\perp^2$ is taken into account. Then, the equation to be solved is [see equations (21) and (23)]

$$(1 - \eta^2)\frac{d^2g}{d\eta^2} - 2N\eta\frac{dg}{d\eta} + 2N\left[\left(\frac{\tilde{\omega}^2}{\Omega_\perp^2}\right)_{\mathrm{c}}(1 + \epsilon) - K(1 - \eta^2)\right]g = 0, \qquad (29)$$

where

$$\epsilon(r) = \frac{\tilde{\omega}^2(r)}{\tilde{\omega}_{\mathrm{c}}^2}\frac{\Omega_{\perp\mathrm{c}}^2}{\Omega_\perp^2(r)} - 1. \qquad (30)$$

The value of ϵ is obviously zero at r_{c}. If we consider the radial dependences of $\Omega_\perp$ and Ω_{K}, we see, after some calculation, that $\epsilon > 0$ for $r < r_{\mathrm{c}}$ and $\epsilon < 0$ for $r > r_{\mathrm{c}}$, when $\omega > 0$. When $\omega < 0$, however, situation is changed and $\epsilon < 0$ for $r < r_{\mathrm{c}}$ and $\epsilon > 0$ for $r > r_{\mathrm{c}}$, as far as a_* is small and $|\omega|$ is not too large.

For the above perturbation method to be valid, the final results must guarantee that $\epsilon(r)$ given by equation (30) is smaller than unity in the trapped region. The final results really show that this is the case.[2] Here, we briefly mention the case of corrugation waves (c-mode oscillations) considered by Silbergleit et al. (2001). The corrugation waves are oscillations of $n = 1$ and $m = 1$. In the case of $n = 1$, $\epsilon(r)$ is reduced to $\epsilon(r) = \tilde{\omega}^2/\Omega_\perp^2 - 1$, since $(\tilde{\omega}/\Omega_\perp)_{\mathrm{c}}^2 = 1$ [see equations (25) and (26)]. Hence, if $m = 1$ we have $\epsilon = (\omega - \Omega)^2/\Omega_\perp^2 - 1$, and $|\epsilon(r)| \ll 1$ is expected if low frequency oscillations are present. Silbergleit et al. (2001) showed that such oscillations are really present. This is trapping of c-mode oscillations. Note, however, that in this paper we are interested in oscillations with $m = 2$, not $m = 1$.

Equation (29) is solved by a standard perturbation method, i.e, the perturbed part of g is expressed by a series of the Gegenbauer polynomials and thier coefficients as well as $K(r)$ are determined from the solvability condition of the inhomogeneous equation, using that the Gegenbauer polynomials, $C_n^\lambda(\eta)$, are orthogonal in the range of (-1,1) with the weight $(1 - \eta^2)^{\lambda - 1/2}$. Considering this, we have, after some calculation,

$$2NK(r) = n(n + 2\lambda)\frac{1}{2}\epsilon(r)\chi(r), \qquad (31)$$

where

$$\chi(r) = \begin{cases} 3\Gamma - 1 & \text{for} \quad n = 1 \\ 2\Gamma(5\Gamma - 4)/(4\Gamma^2 - 7\Gamma + 4) & \text{for} \quad n = 2 \\ (3\Gamma - 1)(7\Gamma - 5)/(6\Gamma^2 - 9\Gamma + 5) & \text{for} \quad n = 3. \end{cases} \qquad (32)$$

4.2 Radial Eigen-Value Problem

The results in the above subsection show that the equation to be solved as the eigen-value problem in the radial direction, i.e., equation (22), is written as

---

[2] For example, in the oscillations of $n = 2$ and $n_{\mathrm{r}} = 0$ (see the next subsection for the meaning of n_{r}) with $\Gamma = 5/3$, the range of variation of $\epsilon(r)$ in the trapped region is $0 \sim 0.12$ ($a_* = 0$) and $0 \sim 0.14$ ($a_* = 0.2$). In the case of $n = 3$ and $n_{\mathrm{r}} = 0$ with $\Gamma = 1.3$, we have $\epsilon = 0 \sim 0.0135$ ($a_* = 0$) and $0 \sim 0.0138$ ($a_* = 0.2$).

(Silbergleit et al. 2001), using equation (12), (25) and (31),

$$\frac{1}{\tilde{\omega}}\frac{d}{dr}\left[\frac{\tilde{\omega}}{\tilde{\omega}^2-\kappa^2}\frac{d\tilde{h}_1}{dr}\right] + \frac{\epsilon\chi}{2c_{s0}^2}\tilde{h}_1 = 0. \tag{33}$$

Now, we introduce a new independent variable $\tau(r)$ defined by

$$\tau(r) = \int_{r_i}^{r}\frac{\tilde{\omega}^2(r')-\kappa^2(r')}{\tilde{\omega}(r')}dr', \quad \tau_c \equiv \tau(r_c). \tag{34}$$

Then, equation (33) is written in the form:

$$\frac{d^2\tilde{h}_1}{d\tau^2} + Q\tilde{h}_1 = 0, \tag{35}$$

where

$$Q(\tau) = \frac{\tilde{\omega}^2}{\tilde{\omega}^2-\kappa^2}\frac{\epsilon\chi}{2c_{s0}^2}. \tag{36}$$

Equations (35) and (36) show that the propagation region of oscillations is the region where $Q > 0$. The region is that of $\epsilon > 0$, which is found to be inside of r_c, when $\omega > 0$. In the case of $\omega < 0$, the propagation region is outside r_c and oscillations are not trapped.

Silbergleit et al. (2001) solved equation (35) by a standard WKB method with relevant boundary conditions. The WKB approximation shows that the solution of equation (35) can be represented as

$$\tilde{h}_1 \propto Q^{-1/4}(\tau)\cos\left[\Phi(\tau)-\Phi_c\right] \tag{37}$$

in the whole capture region $0 < \tau < \tau_c$, except small vicinities of its boundaries of $\tau = 0$ and $\tau = \tau_c$. Here, $\Phi(\tau)$ is defined by

$$\Phi(\tau) = \int_0^{\tau}Q^{1/2}(\tau')d\tau' = \int_{r_i}^{r}Q^{1/2}(r')\frac{\tilde{\omega}^2(r')-\kappa^2(r')}{\tilde{\omega}(r')}dr', \tag{38}$$

and Φ_c is a constant to be determined by boundary conditions. Concerning the outer boundary condition, they take into account that the capture radius, r_c, is a turning point of equation (35) since the sign of ϵ changes there. The inner boundary condition adopted is vanishing of an arbitrary combination of $\tilde{h}_1$ and $d\tilde{h}_1/dr$ at r_i. In their treatment, r_i is taken at the marginary stable radius and $1/c_{s0}$ is assumed to have a weak singularity at the radius as $1/c_{s0} \propto (r-r_i)^{-\mu}$ with an arbitrary parameter μ. In realistic disks, however, the inner edge is not a singularity but the temperature and density continue smoothly inward. Considering this and for simplicity, we adopt $\mu = 0$. Furthermore, we consider only the case of $\tilde{h}_1 = 0$ or $d\tilde{h}_1/dr = 0$ at the inner boundary. Then, their results of WKB analyses show that the trapping condition is

$$\int_0^{\tau_c}Q^{1/2}d\tau = \begin{cases} \pi(n_r+1/4) & \text{for} \quad d\tilde{h}_1/dr = 0 \\ \pi(n_r+3/4) & \text{for} \quad \tilde{h}_1 = 0, \end{cases} \tag{39}$$

9

where $n_r(= 0, 1, 2, ...)$ is zero or a positive integer specifying the node number of $\tilde{h}_1$ in the radial direction. The constant Φ_c is also determined as

$$\Phi_c = \begin{cases} 0 & \text{for} \quad d\tilde{h}_1/dr = 0 \\ \pi/2 & \text{for} \quad \tilde{h}_1 = 0. \end{cases} \tag{40}$$

For a given set of parameters, including spin parameter a_*, polytropic index N, and mass of neutron stars, M, any solution of equation (39) specifies r_c, which gives ω of the trapped oscillation through equation (25). In other words, ω and r_c are related by equation (25), i.e., $\omega = \omega(r_c)$ or $r_c = r_c(\omega)$. Then, the trapping condition determines r_c or ω as functions of such parameters as a_* and N.

5 Numerical Results

To obtain numerical values of the frequency, ω, and the capture radius, r_c, of trapped oscillations, we must specify the radial distribution of acoustic speed, i.e., $c_{s0}(r)$. Since the final results of numerical calculations depend only weakly on the radial dependence of c_{s0}, we adopt the temperature distribution in the standard disk, where gas pressure dominates over radiation pressure and opacity mainly comes from the free-free processes, which is (e.g., Kato et al. 2008)

$$c_{s0}^2 = 1.83 \times 10^{16} \Gamma (\alpha m)^{-1/5} \dot{m}^{3/5} r^{-9/10} \text{ cm}^2 \text{ s}^{-2}, \tag{41}$$

where α is the conventional viscosity parameter, $m(\equiv M/M_\odot)^3$ and $\dot{m} = \dot{M}/\dot{M}_{\text{crit}}$, $\dot{M}_{\text{crit}}$ being the critical mass-flow rate defined by

$$\dot{M}_{\text{crit}} \equiv \frac{L_E}{c^2} = 1.40 \times 10^{17} m \text{ g s}^{-1}, \tag{42}$$

where L_E is the Eddington luminosity. Parameters α and $\dot{m}$ affect on the frequencies of trapped oscillations only through the magnitude of c_{s0}. We adopt, throughout this paper, $\alpha = 0.1$ and $\dot{m} = 0.3$. Other parameters specifying the disk-star system are $m(\equiv M/M_\odot)$ and a_*. We consider the cases of $m = 2.0$ and $a_* = 0 \sim 0.3$.

We only consider two-armed oscillations with one, two, or three node(s) in the vertical direction, i.e., $n = 1$, 2, or 3.[4] Oscillations with more nodes in the vertical direction are less interesting from the view point of observability. The inner boundary of oscillations is taken at the radius of $\kappa = 0$, i.e., at the radius of the marginally stable circular orbit. At the radius, we impose $\tilde{h}_1 = 0$ as the

---

[3] In this section and hereafter, m is often used to denote $M/M_\odot$ without confusion with the azimuthal wavenumber m of oscillations.

[4] In oscillations with odd number of n, $h_1(r, z)$ is antisymmetric with respect to the equatorial plane. That is, in oscillations with $n = 3$, for example, h_1 have one node between the equator and the disk surface except on the equator. See the functional form of g given in equation (28).

boundary condition[5] except in figure 5, where $d\tilde{h}_1/dr = 0$ is also considered as the boundary condition at r_i, for comparison. The horizontal node number, n_r, of oscillations we consider is mainly $n_r = 0$ and supplementally $n_r = 1$ and 2.

Figures 1 and 2 are the propagation diagrams for oscillations of $n = 1$ and 2 (figure 1) and $n = 3$ (figure 2), respectively. Only the oscillations of $n_r = 0$ and $\Gamma = 5/3$ are shown in figure 1, but three modes of oscillations, i.e., $n_r = 0$, 1, and 2, are shown in figure 2 for the case of $\Gamma = 1.25$. In the cases of figure 1, the propagation regions of oscillations on the frequency-radius diagram are below the curves of $2\Omega - \Omega_\perp$ and $2\Omega - (1+\Gamma)^{1/2}\Omega_\perp$ for $n = 1$ and $n = 2$, respectively. The results of numerical calculations show that the oscillations of $n = 1$ and $n_r = 0$ are trapped in the radial range shown by the upper thick horizontal line in figure 1. The frequency ω and the capture radius r_c are, respectively, $\omega = 864$Hz and $r_c = 3.53r_g$. Outside r_c, the oscillation is spatially damped. The radial range of trapped oscillations with $n = 2$ and $n_r = 0$ is shown by the lower thick horizontal line in figure 1. The frequency and the capture radius in this case are $\omega = 298$Hz and $r_c = 3.69r_g$.

Trapped oscillations of $n = 3$ have frequencies lower than those of $n = 1$ and 2, since on the propagation diagram the curve of $2\Omega - (3\Gamma)^{1/2}\Omega_\perp$ is below those of $2\Omega - \Omega_\perp$ and $2\Omega - (1+\Gamma)^{1/2}\Omega_\perp$ (compare figures 1 and 2). It should be noted that the oscillation modes with $n = 3$ cannot be trapped if $\Gamma \geq 4/3$, since in this case the propagation region is unbounded outside and the oscillations can propagate away infinity as shown by arrow (see the curve of $2\Omega - (3\Gamma)^{1/2}\Omega_\perp$ for $\Gamma = 1.45$ in figure 2). In figure 2, the frequency and the radial extend of trapped oscillations with $n = 3$ are shown for $\Gamma = 1.25$ for three modes concerning the radial direction; the fundamental mode (i.e., $n_r = 0$) and the first two overtones (i.e., $n_r = 1$ and 2). The sets of frequency and capture radius for these three modes of $n_r = 0$, 1, and 2 are, respectively, $(40.8$Hz, $4.30r_g)$, $(25.8$Hz, $5.84r_g)$, and $(17.2$Hz, $7.66r_g)$.

Figure 3 shows the Γ-dependence of the capture radius r_c. As a typical case, the dependence is shown for oscillations with $n_r = 0$ and some values of n. It is noted that when Γ is close to $4/3$, the capture radius of oscillations with $n = 3$ is far outside and their frequencies are low. These characteristics become more prominent for oscillations with $n_r \geq 1$, although they are not shown in figure 3 (see figure 5).

The frequency-Γ relations are summarized in figure 4 for a few modes of oscillations in two cases of $a_* = 0$ and $a_* = 0.1$. Modes of oscillations adopted are $n = 1$, 2, and 3. In all cases n_r is taken to be $n_r = 0$. As mentioned before, the oscillations with $n = 3$ have low frequencies. In order to examine characteristics of these low frequency oscillations more in detail, the frequency-

---

[5] If we assume that the Lagrangian variation of pressure, i.e., δp, vanishes at $r = r_i$, the condition of $h_1 = 0$ at $r = r_i$ will be a better approximation than $\partial h_1/\partial r = 0$ at $r = r_i$ by the following reasons. The Lagrangian variation of pressure, δp, can be expressed as $\delta p = \rho_0 h_1 + \xi_r \partial p_0/\partial r + \xi_z \partial p_0/\partial z$, where ξ_r and ξ_z are, respectively, the radial and vertical displacements associated with the perturbation and related to u_r and u_z by $i(\omega - m\Omega)\xi_r = u_r$ and $i(\omega - m\Omega)\xi_z = u_z$, respectively. If we consider that equations of motion, equations (14) – (16), and that the pressure will not change so sharply at the r_i, the major term among the above expression for δp will be $\rho_0 h_1$.
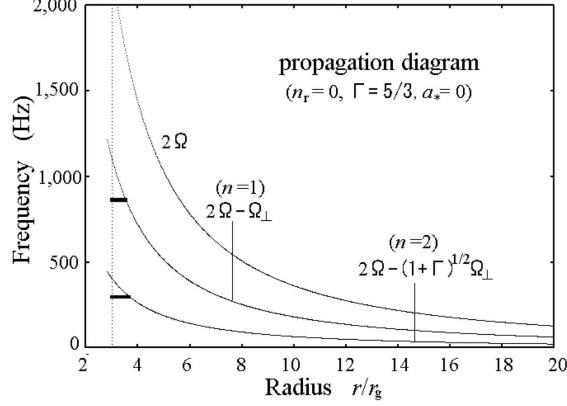
Figure 1: Frequency - radius plane (i.e., propagation diagram) showing the propagation region of two-armed nearly vertical oscillations. The propagation region of oscillation modes with $n = 1$ is below the curve labelled by $2\Omega - \Omega_\perp$, and the trapping of the oscillations with $n = 1$ and $n_r = 0$ is shown, in the case of $\Gamma = 5/3$, by the upper thick horizontal line (frequency is ~ 864Hz and capture radius is $\sim 3.53r_g$). In oscillations with $n = 2$, the curve specifying the boundary of the propagation region, i.e., $2\Omega - (1 + \Gamma)^{1/2}\Omega_\perp$, depends on Γ, and the curve for $\Gamma = 5/3$ is shown. The propagation region of oscillations with $n = 2$ is below this curve in the case of $\Gamma = 5/3$. For $\Gamma = 5/3$, the trapping of the oscillations with $n = 2$ and $n_r = 0$ is shown by the lower thick horizontal line (frequency is ~ 298Hz and capture radius is $\sim 3.69r_g$). The inner boundary condition adopted at r_i is $\tilde{h}_1 = 0$. This inner boundary condition is adopted in all cases in this paper, except for in figure 5. The central star is assumed to have no spin. The mass of the central star is taken to be $2M_\odot$ in all cases shown in figures in this paper.

Γ relation in case of $n = 3$ is again shown in figure 5, including cases where other parameter values are adopted. That is, in addition to oscillations with $n_r = 0$, oscillations with $n_r = 1$ and 2 are considered in figure 5. In addition, the cases where $d\tilde{h}_1/dr = 0$ is adopted as the inner boundary condition at r_i are shown by thin curves. In figure 6, the frequency - spin relation is shown for three modes of oscillations with $n = 1$, 2, and 3, where $n_r = 0$ and some values of Γ are adopted.

6 Discussion

In this paper we have examined characteristics of two-armed ($m = 2$), nearly vertical oscillations, assuming that the disk consists of barotropic gases with polytropic index Γ. The parameters specifying oscillation modes are n and
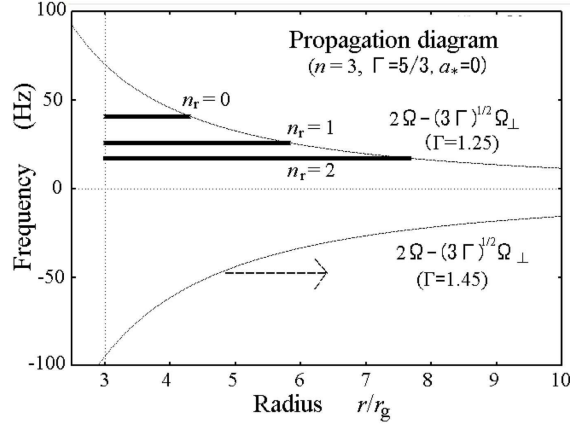
Figure 2: The same as figure 1, except that the oscillations with $n = 3$ are considered here. The propagation region of the oscillations is below the curve labelled by $2\Omega - (3\Gamma)^{1/2}\Omega_\perp$, and the curve in the case of $\Gamma = 1.25$ is shown. Trapping of three modes of oscillations with $n_r = 0$, 1, and 2 are shown by three horizontal thick lines. The sets of frequency and capture radius for these three oscillation modes are, in turn, (40.8Hz, $4.30r_g$), (25.8Hz, $5.84r_g$), and (17.2Hz, $7.66r_g$). For the gas with $\Gamma > 4/3$, the propagation region is in the outer region of disks, which is shown by arrow, and there is no trapping.
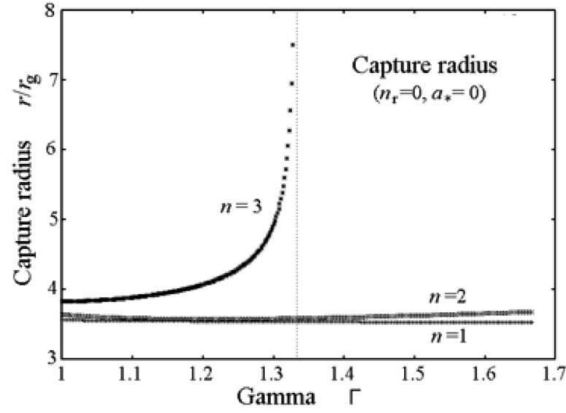

Figure 3: Capture radius, r_c, as functions of Γ for three modes of $n = 1$, 2, and 3. The radial node number n_r is taken to be zero with boundary condition $\tilde{h}_1 = 0$ at $r_i = 3r_g$, the spin parameter being $a_* = 0$. In oscillations with $n = 3$, the trapping is absent for $\Gamma > 4/3$, when $a_* = 0$.
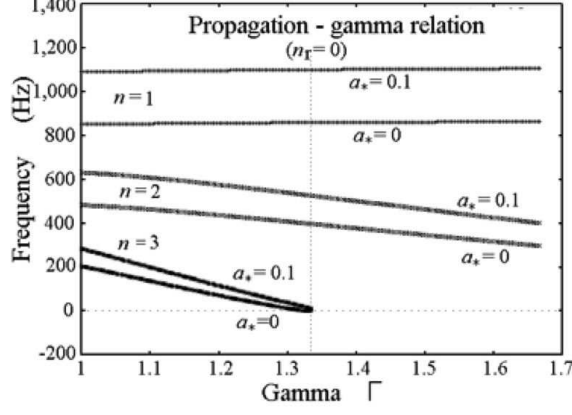
13

Figure 4: Frequency-Γ relation of trapped oscillations for some values of vertical node number n and spin parameter a_*. The oscillations with no node in the radial direction ($n_r = 0$) are considered with boundary condition of $\tilde{h}_1 = 0$ at r_i.
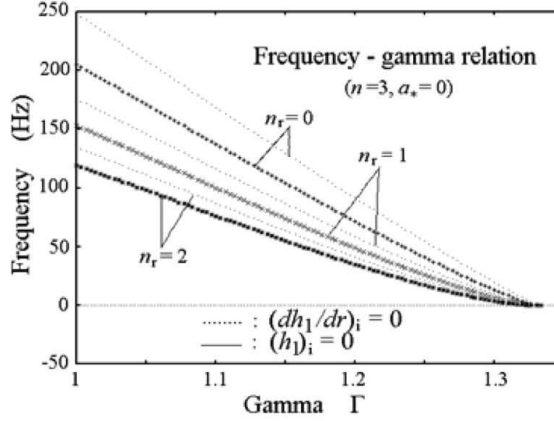

Figure 5: Frequency-Γ relation for oscillation modes with $n = 3$. Effects of differences of radial node number n_r and of boundary condition on the frequency of trapped oscillations are examined. Two cases of boundary conditions, $\tilde{h}_1 = 0$ and $d\tilde{h}_1/dr = 0$ at r_i, are compared for three modes of oscillations with radial node number $n_r = 0$, 1, and 2. The thick curves are for the cases where the inner boundary condition is taken as $\tilde{h}_1 = 0$, while the thin curves are the cases of $dh_1/dr = 0$. The spin parameter a_* is taken to be zero.
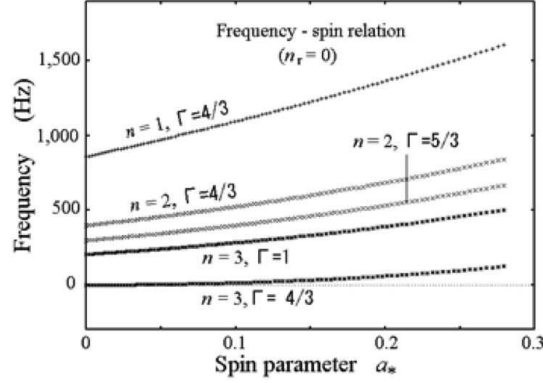
14

Figure 6: Frequency-spin relation for modes with $n = 1$, 2, and 3. The radial node number is taken to be $n_{\rm r} = 0$.

$n_{\rm r}$, where $n(= 1, 2, 3...)$ is the node number of h_1 in the vertical direction, and $n_{\rm r}(= 0, 1, 2, ...)$ is the node number of h_1 in the horizontal direction. An additional important parameter is Γ, which is especially important in oscillations with $n = 3$. Main results obtained are i) there are oscillation modes that are trapped in the inner region of disks, and ii) their frequencies depend on modes of oscillations $(n, n_{\rm r})$ and Γ, and cover a wide range of frequency. That is, the trapped oscillations of $n = 1$ and 2 have frequencies of the order of kHz QPOs, and those of $n = 3$ are in the frequency range of the horizontal-branch QPOs (HBQPOs).

One of interesting characteristics of the oscillations is that their frequencies can change rather widely by change of disk structure, which is distinct from the g-mode oscillations trapped around the radius of $\kappa_{\rm max}$ (Okazaki et al. 1987), where $\kappa_{\rm max}$ is the maximum value of the epicyclic frequency. That is, as shown in figure 4, the frequencies of trapped oscillations decrease by increase of Γ, in the $n = 2$ and $n = 3$ modes. In the $n = 1$ modes, however, their frequencies are insensitive to a variation of Γ (see figure 4). This can be easily understood if we consider the Γ-dependence of the boundary curve specifying the capture radius on the propagation diagram [see figures 1 and 2, and also equations (6) and (7)].

In this paper we did not quantitatively consider the effects of $c_{\rm s0}(r)$ on frequency. An increase of $c_{\rm s0}$ without any change of other parameters leads to decrease of frequency of trapped oscillations. The reason is that an increase of $c_{\rm s0}$ decreases Q. Hence, to satisfy the trapping condition (39), an increase of $r_{\rm c}$ is necessary, which leads to decrease of frequency (see figures 1 and 2). In table 1, the effects of changes of various parameter values on frequencies of trapped oscillations are summarized.

One of important problems remained is whether the nearly vertical oscilla-

15

Table 1: table 1.

parameters		frequency
parameters of oscillations	increase of n (except for $n = 1$)	decrease
	increase of n_{r}	decrease
disk parameters	increase of Γ (except for $n = 1$)	decrease
	increase of c_{s0}	decrease
parameters of stars	increase of $m \equiv (M/M_{\odot})$	decrease
	increase of a_*	increase

tions considered in this paper can be really excited on disks. Two possibilities will be conceivable. One is the excitation by the process of viscous overstability of oscillations (Kato 1978). This, however, might be inefficient to some types of oscillations, especially to oscillations with large n. Another and more promising process is the stochastic excitation of oscillations by turbulence, developed first by Goldreich and Keely (1977a,b). This is known as the excitaion process of solar and stellar non-radial oscillations. This process is better than the former in the sense that it will be able to excite many types of oscillations, without no particular selection concerning the forms of eigenfunctions.

So far, we did not discuss the effects of corotation resonance on the present trapped oscillations. It is known that non-axisymmetric g-mode oscillations are generally damped by corotation resonance (Kato 2003; Li et al. 2003; Latter & Balbus 2009; see also Silbergleit & Wagoner 2008). The c-mode oscillations, which are non-axisymmetric, are also damped by the resonance (Tsang & Lai 2009). These results are related to the fact that these oscillations have node(s) in the vertical direction. The vertical oscillations considered in this paper have also node(s) in the vertical direction. The oscillations, however, have an important difference from g- and c-mode oscillations. That is, in the case of two-armed nearly vertical oscillations, the radius of coratation resonance, i.e., the radius where $\omega = 2\Omega$ is realized, is far outside the propagation region (see the curve of 2Ω in figure 1; the curve of 2Ω is not shown in figure 2, since it is outside the diagram). In the evanescent region the wave amplitude is spatially damed exponentially. Hence, the effects of corotation damping are negligible in the present oscillations.

It will be important to note here that the effects of the general relativity are not essential in the trapping of the present vertical oscillations, except for the modes with $n = 1$. The propagation region of the vertical oscillations is specified by inequality (8). In deriving inequality (8), the fact that $\Psi_n \Omega_{\perp}^2$ is larger than κ^2 is adopted. In the case of oscillation modes of $n = 1$, the general relativity is necessary to guarantee this, since $\Psi_n = 1$. In oscillations with $n \geq 2$, however, $\Psi_n \Omega_{\perp}^2 > \kappa^2$ is guarantees even in Newtonian disks. Other important ingredients for presence of trapped oscillations are the presence of inner edge of disks where waves are reflected back and a monotonical decrease of angular

velocity of rotation, $\Omega(r)$, outwards. This point is different from trapping of g-mode oscillations, since in trapping of g-mode oscillations, the general relativity is essential. If we want to describe the QPOs in disks extending from black-hole or neutron star systems to dwarf-novae systems by a common mechanism, the nearly vertical oscillations considered here will be one of good candidates, since in the disks of dwarf-novae the effects of the general relativity are minor.

We have shown that there are various modes of nearly vertical oscillations trapped in the inner region of disks. From the observational points of view, however, the oscillations with $n = 1$ and $n = 2$ may not be so interesting, since their trapped regions are too narrow as shown in figures 1 and 3, and may not be observed with large amplitudes, although the trapped regions are close to the inner edge of disks. Compared with them, the oscillations with $n = 3$ will be of interest, since their trapped region is wide as shown in figures 2 and 3. In this sense, the $n = 3$ modes will be one of possible candidates of low frequency QPOs such as horizontal-branch QPOs (HB QPOs). Further discussion on this direction will be worthwhile. Related to this, there are some issues to be noted here.

First, we have found that low frequency oscillations with $n = 3$ are present only in disks with $\Gamma < 4/3$. Hence, one may imagine that such oscillations cannot be expected in neutron-star disks, since the standard disk model shows that the main part of the disks is gas-pressure-dominated. We should notice, however, that in disks with high accretion rate (accretion rate is close to or higher than the critical accretion rate defined by the Eddington luminosity), a radiation-pressure-dominated region appears in the innermost part of disks. In particular, in slim disks the whole region is radiation-pressure-dominated. Furthermore, we should notice that it is unnecessary to regard the index Γ as the same as the ratio of the specific heats, γ, of the disk gas. In practice, we can expect $\Gamma < \gamma$ by the following reasons. Due to radiation from a hot corona, disks have tendency to approach isothermal disks in the vertical direction. Furthermore, in low frequency oscillations, radiative heat transport tends to make the oscillations isothermal, although as another effect it may dampen oscillations.

Second, the oscillations with $n = 3$ are trapped in a rather wide region,, i.e., the radial wavelength is long. Hence, it will be necessary to take into account some terms neglected in deriving equation (19), including the terms of relativistic corrections, when we want to do more quantitative estimate of oscillation frequencies.

Finally, we should mention a difference between the low frequency oscillations with $n = 3$ discussed in this paper and the low-frequency one-armed corrugation waves (Kato 1989, Silbergleit et al. 2001). The latter oscillations are a kind of warps or tilts, and roughly an incompressible deformation of disks, while the former are compressible oscillations.

References

Ferreira, B.T. & Ogilvie, G.I. 2008, MNRAS, 386, 2297

Goldreich, P. & Keely, D.A. 1977a, ApJ, 211, 934

Goldreich, P. & Keely, D.A. 1977b, ApJ, 212, 243

Henisey, K.B., Blaes, O.M., Fragile, P.C., & Ferreira, B.T. 2009, arXiv:0910.1882
    (to be published in ApJ)

Kato, S. 1978, MNRAS, 185, 629

Kato, S. 2001, PASJ, 53, 1

Kato, S. 2003, PASJ, 55, 257

Kato, S. 2004, PASJ, 56, 905

Kato, S. 2005, PASJ, 57, 699

Kato, S. 2008a, PASJ, 60, 111

Kato, S. 2008b, PASJ, 60, 1387

Kato, S., Fukue, J. 2006, PASJ, 58, 909

Kato, S., Fukue, J., & Mineshige, S. 2008, Black-Hole Accretion Disks — To-
    wards a New paradigm — (Kyoto: Kyoto University Press)

Latter, H.N. & Balbus, S.A. 2009, MNRAS, 399, 1058

Li, L.-X., Goodman, J., Narayan, R. 2003, ApJ, 593,980

Nowak, M.A & Wagoner, R.V. 1992, ApJ, 393, 697

Okazaki, A.T., Kato, S., & Fukue, J. 1987, PASJ, 39, 457

Oktariani, F., Okazaki, A.T. & Kato, S. 2010, submitted to PASJ

Perez, C.A., Silbergleit, A.S., Wagoner, R.V., & Lehr, D.E. 1997, ApJ, 476, 589

Silbergleit, A.S., Wagoner, R., & Ortega-Rodriguez, M. 2001, ApJ, 548, 335

Silbergleit, A.S. & Wagoner, R. ApJ, 680, 1319

Tsang, D. & Lai, D. 2009, MNRAS, 393, 992